Phase transitions in stigmergic territorial systems

A. Heiblum Robles and L. Giuggioli
Bristol Centre for Complexity Sciences and Department of Engineering Mathematics, University of Bristol, Bristol, BS8 1UB
(Dated: September 6, 2018)

A mechanism to generate spatially segregated territories in 2D consists of individuals depositing their own marks and avoiding foreign ones. This form of environment-mediated interaction, called stigmergy, makes the emerging spatio-temporal territory dynamics quite rich. Short-lived marks produce rapidly morphing and highly mobile territories. Long-lived marks yield slow territories with a narrowly defined shape distribution. The change in territory mobility depending on the time for which individual marks remain active is accompanied by a liquid-hexatic-solid transition akin to the Kosterlitz-Thouless melting scenario.

PACS numbers: 64.70.-p, 87.10.Hk, 05.65.+b, 05.40.Fb
Keywords: Animal territoriality, phase transitions, ecology, territorial random walk

INTRODUCTION

Coordinating the activity of multiple agents in a decentralized manner is the aim of a variety of man-made systems [1] and the intrinsic occurrence in natural systems [2]. When coordination is achieved by relying on information residing external to the agents, individuals are said to interact indirectly. If the space retains memory of the passage or activity of an agent, the indirect interaction between individuals is mediated by the environment. This general phenomenon, called stigmergy [3], was coined in the '50s to explain nest building in termites [4]. Since then the term has been employed to explain the spontaneous emergence of coordinated activities and complex patterns beyond the realm of biology. It has inspired a variety of algorithms to solve distributed control and optimization problems [5], e.g. packet routing along communication networks [6], multi-robot construction [7] and search tasks [8].

Besides the collective coordination in complex tasks, stigmergic processes may also serve the purpose of directing individuals towards or away from certain regions of space. Ant exploration of new areas following the pheromone trails left by others is an example of movement towards a goal [9]. Ant fleeing from alarm pheromones deposited to signal the presence of danger is an example of a movement to avoid certain locations [9]. Avoidance behaviour, specifically eschewing marks deposited by others, is also the behaviour with which territorial patterns of various vertebrates form. Spatial segregation in minimally overlapping regions is accomplished by individuals leaving their own marks wherever they go, while retreating upon encountering foreign ones. Although there exist cases of such behaviour in humans, e.g. the dynamics of street gangs and their use of graffiti for territorial marking [10], many examples are found in the animal kingdom. The collective formation of territories in scent-marking animals, studied mathematically since the '90s [11–13], has recently been shown to possess all the salient characteristics of stigmergy [14].

The ubiquity of stigmergic territorial systems prompts the question of what are the local interaction mechanisms that have significant impact on the formation of patterns at larger scales. Inspired by investigations in other forms of animal collective movement where, differently from our case, alignment plays a fundamental role [15–18], we determine whether the system undergoes any structural change as a function of the individual avoidance behaviour. To investigate the existence of order-disorder phase transitions we borrow from studies in a broad range of 2D materials where the transition from a disordered fluid to an ordered solid has been the subject of long lived debate. Such transition may be quite complex with the appearance of a partially ordered phases, called "hexatic", due to the importance of geometrical arrangements of the first 6 neighbours, as supported by the KTHNY theory of melting [19–21].

TERRITORIAL RANDOM WALKERS AND SPATIAL COMPETITION

For our investigation we use the so-called territorial random walk (TRW) model, a collective movement model introduced by one of the present authors in the past [22], and tested with empirical observations of a red fox population [23], a scent-marking territorial species. The TRW model consists of interacting random walkers moving on a lattice with periodic domains where each site visited is scent-marked. The scent-marks are not permanent but they vanish after a designated active time T_A from deposition. Foreign scent-marks function as a movement deterrent forcing other walkers to retreat upon their encounter. In this way walkers interact indirectly by modifying the environment upon their passage. This stigmergy generates regions of space, the territories, that are of exclusive use to the walker who scent-marked them, except at the borders when neighbouring territories may overlap. As the information of the passage of an individual is lost after time T_A, a territory at any time t is

defined as the set of all sites visited by the same individual in the interval $(t - T_A, t)$.

Space competition drives the dynamics of the territories and can be measured by the strength with which a walker exerts pressure on its neighbours while the locations visited by an individual represent movement barriers. This strength can be estimated by comparing the average space available per individual to the space a walker would occupy in the absence of other walkers within time T_A. The former is determined by the inverse of the population density, or specific volume, $\nu = L^d/N$ with N the number of walkers, and L^d the number of sites in the d-dimensional lattice. The latter is estimated with the average number S_n of distinct sites visited by a single walker after n jumps up to time T_A. With the walkers performing jumps at rate F we take $n = FT_A$ and notice that (see Supplementary Section) $S_n = Cn^{0.91}$ with C a constant dependent on the geometry of the lattice. We define the ratio

$$Z = S_n/\nu, \tag{1}$$

as the spatial competition parameter. This dimensionless quantity has the advantage of being appropriate to any number of dimensions. As the hexagonal tessellation is the geometrical arrangement that minimizes surface tension, we have chosen a triangular lattice ($C = 0.73$) to avoid introducing spatial frustration effects.

Discarding finite size effects, the physics are fully determined by the pair ν and FT_A, or equivalently, by ν and Z. Although the definition of Z includes ν, this pair of parameters is preferable as it simplifies the analysis, as Z itself is some sort of measurement of the interaction. It compares the space that a non-interacting walker occupies (S_n) with the average space available (ν). For $Z \lesssim 1$ walkers rarely encounters foreign scent and have the sufficient space to expand. The system behaves fundamentally as an ensemble of non-interacting walkers. On the other hand, $Z \gtrsim 1$ implies that walkers have on average less space than necessary, so they are in a constant struggle to expand exterting 'pressure' on the territory boundaries. This can be captured by measuring the distribution of territory sizes.

A meaningful quantity to plot is the standard deviation of territory size divided by its mean. Such curve displays a non-monotonic curve with a clear maximum. This maximum can be thought of as the transition between low-interaction and high-interaction regimes. To the left of the maximum, the small size of the territories is what constrains the possible variations between them, and thus the variance of the distribution. To the right, the interaction imposes an order into the system. The constant interaction of the walkers with the boundaries of neighbouring territories prevents them from diffusing further and the trajectories become more recurrent. This has the effect of more rounded or convex territories and reduced territory size variance.

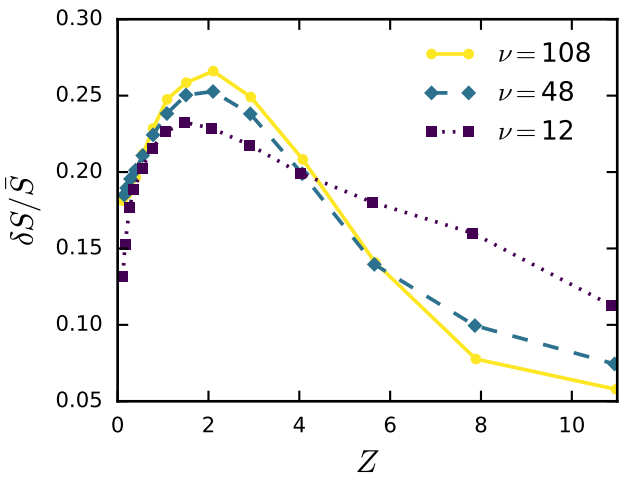

FIG. 1. (Color online) Standard deviation of the territory size S_d normalised with the mean territory size $\bar{S}$ as a function of the spatial competition parameter Z. To the left of the maximum, the interaction is weak and territory size tends to be independent. To the right of the maximum the interaction dominates and all territories become more homogeneous both in size and shape.

Each curve of Fig 1 was generated as follows. First, to reduce the parameter space and simplify the analysis, we constrain it to the case $F = 1$ (arb. units), that is, walkers can jump 1 site per time step. A simulation with fixed ν and T_A was started either from random initial conditions or from a hexagonal tessellation. After a sufficiently large thermalisation time (see below for further details) a snaptshot is taken from the system and each territory size is measured. From this snapshot the territory size distribution is built and the standard deviation is measured. This value could be improved by repeating the process and taking the ensemble average, however, thanks to the self-averaging effect of the system the results obtained from one sample are sufficiently accurate. This procedure yields one dot of Fig 1. This procedure is repeated for different values of ν and T_A. The values of ν where restricted to allow the territories to adopt hexagonal shapes. Next, all the dots sharing the same ν were connected graphically to create the displayed curves.

While we emphasize the role of Z it is not sufficient to characterise the phenomena observed. In general, two systems with the same Z but different ν are in different, although similar, states. For larger values of ν, that is for less dense systems, the difference becomes less noticeable but good quality results become expensive computationally at a rate exponentially proportional to ν. In what follows only the case $\nu = 48$ is explored and other cases are left for furture analysis.

STOCHASTIC SIMULATIONS

Large numerical simulations were run to explore the different spatial configurations displayed by the model. Several combinations of the number of animals N and the number of sites in the grid $L \times L$ were chosen such that the ratio between them was $\nu = 48$. The largest pair of values chosen were $N = 132,300$ and $L^2 = 2520^2$ and the second largest $N = 30,000$ and $L^2 = 1200^2$. The values of T_A were taken in the range $[0, 1513]$, which implies $Z \in [0, 12]$. Simulations were started from both random initial conditions (i.e. walkers start at random sites with no prior scent profile whatsoever) and from a hexagonal tessellation (each walker is given an initial scent profile of hexagonal shape and the aggregation of all territories tessellates the space). Simulations were left to run until the values of all observables converged regardless of the initial condition. Then data was collected to be analysed. Depending on the value of T_A, this "thermalisation" procedure usually took several months running on a high performance cluster. Because not all the simulations with $L^2 = 2520^2$ were able to reach this equilibrium, with the exception of Fig. 2 the analysis here presented is with the data set of $L^2 = 1200^2$. Nevertheless we point out that the largest system was very close to equilibrium and displayed very similar results to what is shown here.

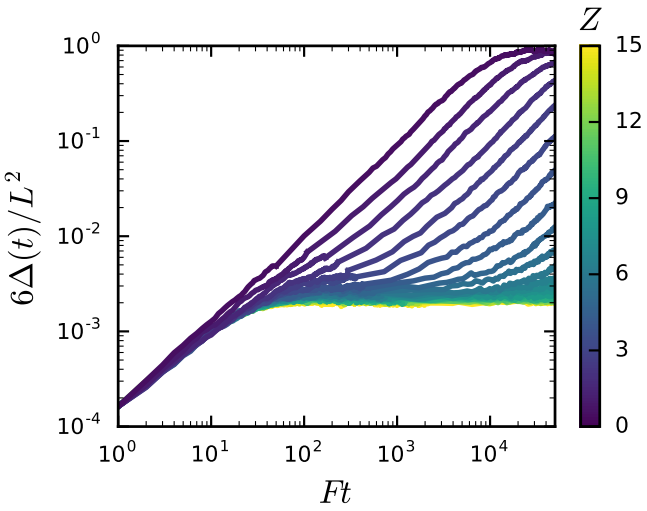

FIG. 2. (Color online) Mean square displacement Δ of a random walker in the 2D TRW model as a function of the dimensionless time Ft for different values of the spatial competition parameter Z for a system with $\nu = 48$ and $L^2 = 192 \times 192$. The different values of Z were obtained by varying only T_A. With the lowest and largest value of Z, the rescaled active time FT_A is, respectively, $n = 50$ ($Z = 0.5$) and $n = 1980$ ($Z = 15.3$).

WALKER SPATIO-TEMPORAL DYNAMICS

To provide the reader with some intuition about the effects of the spatial competition Z on the walker dynamics, we plot in Fig. 2 the mean square displacement (MSD), $\Delta(t) = \langle(\vec{x}(t) - \langle\vec{x}(t)\rangle)^2\rangle$, where $\langle ...\rangle$ represents an ensemble average and $\vec{x}(t)$ is a walker position on the lattice. We show this on an small system to be able to capture accurately all the dynamics, both at short and long scales. At short times the MSD is that of an independent random walker and has the same linear dependence for all Z values. At long times the MSD is normalised to $L^2/6$, the saturation value for an independent random walker in an observation window of size $L \times L$ [24]. In the absence of such window, the walkers would recover a diffusive behaviour as expected from theoretical studies on the so-called fence hindered random walkers, that is walkers that move between partially permeable barriers [25].

Increase in Z triggers a variation in the diffusing behaviour of the walkers, whereby neighbouring individuals exert a 'caging' effect. This caging, reflected into a flattening of the MSD at intermediate times, represents spatial segregation and manifests for longer the larger the competition parameter. Although segregation is only partial as walkers do not remain trapped forever because of the transient nature of the deposited scent, it is evident from the logarithmic time axis that as Z approaches 10 or more, the walkers may remain trapped for extremely long times. In light of this observation and in analogy to phenomena occurring in material science, we expect that different diffusion behaviours of interacting particles can be associated to distinguish between solids and other phases of a system [26]. We do so in the next section.

COARSE GRAINING FROM MARKOV TO NON-MARKOV

To quantify the excluded volume interactions responsible for the caging effect it is convenient to coarse-grain the description of the system. We decrease the spatial resolution and time-integrate the temporal information by neglecting the walkers and considering only the territories over a T_A time-scale. The dynamics of the territories is further simplified by approximating their location and their shape with a centroid and a disk whose size equals the number of lattice sites with an active scent-mark. In so doing we move from a non-Markov microscopic description of the TRW model to a Markov mesoscopic representation of moving and interacting circular particles of variable dimensions. The supplementary Video SV1 shows pictorially this spatio-temporal upscaling. The spatial scale $2\sigma = a\sqrt{\nu}$, where a is the lattice constant, arises naturally as it represents the distance 2σ between evenly spaced centroids when hexagonal territo-

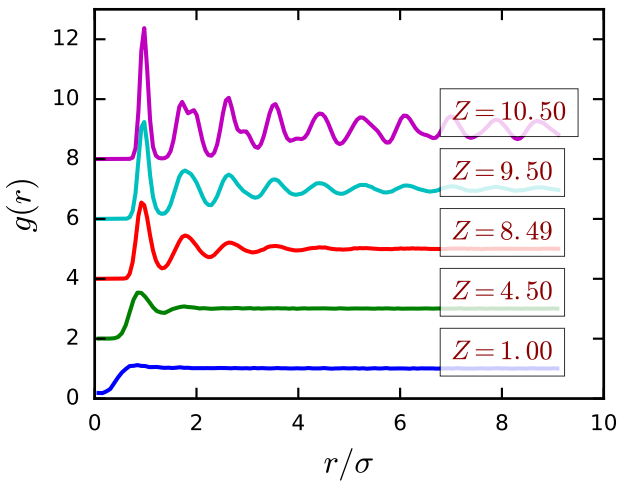

FIG. 3. (Color online) Centroid pair correlation function $g(r)$ for a system with $\nu = 48$ and $L^2 = 1200 \times 1200$ and different T_A. The centroids represent the centre of mass of the territories. The $g(r)$ function represents the probability of finding two particles at a distance r, relative to that of an ideal gas. For ease of visualization each of the top curves have been shifted upwards from zero.

ries tessellate the entire domain (see explicit calculation in Appendix C).

The centroids inherit the diffusive nature of the walkers and are subject to an effective repulsive interaction whose strength depends on the spatial competition. With low Z walkers seldom encounter foreign scent and territories display a wide variety of shapes, which can also be concave. When the centroids of neighbouring territories get very close to each other the approximating circular extended particles may have large part of their areas overlapping one another. As the probability of finding two centroids at small separation is non-zero, the effective exclusion interaction is weak. With high Z, on the other hand, the walkers encounter foreign scent more frequently and territory shapes are more convex. In this case it is unlikely to find two neighbouring centroids closer than a distance 2σ. The effective interaction is strong and constraints the distribution of distances between centroids, ultimately leading to a spatial ordering of the system. The existence of an ordered state in systems with exclusion interactions is well known and results from the emergence of attractive entropic forces [27].

TERRITORY SPATIAL DISTRIBUTION

To identify when different phases in the TRW model appear we characterize the spatial distribution of the centroids at position $\vec{r}_i$ as a function of Z. We do so by first plotting in Fig. 3 the pair correlation function [28], $g(r) = \nu\langle\sum_{i\neq 0}\delta(|\vec{r} - \vec{r}_i|)$, with δ the Dirac's delta function, as a function of the centroid distance $r = |\vec{r}|$ for different Z values. In an ideal gas, the pair correlation function is equal to one as the constituent particles do not interact with each other. In the territorial system that case corresponds to when $Z = 0$. Zones of exclusion are represented by a drop in the $g(r)$ function. When the exclusion is complete, e.g. hard core interaction, the $g(r)$ function is zero for all r within the interaction radius. If the exclusion is not complete, $g(r)$ is small but not zero for small r. The effective interaction between two territories can be thought as hard core for short distances as all pair correlation functions remain relatively flat and almost zero for $r/2\sigma < 1$. However, when Z is small and the territorial system is structureless, $g(r)$ increases from zero to one gradually as exemplified by the bottom line of Fig. 3.

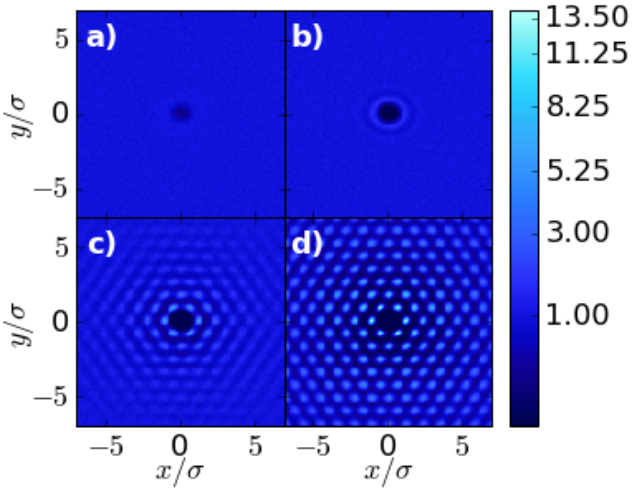

FIG. 4. (Color online) 2D pair correlation function for a 48×10^{-4} size subset of a system with $L^2 = 1200 \times 1200$ and $\nu = 48$. The competition parameters are, respectively, (a) $Z = 1.0$, (b) $Z = 7.25$, (c) $Z = 9.5$, and (d) $Z = 10.25$ and are varied by changing T_A. The vertical gray bar (colored in the online version) indicates the probability density of finding two particles separated by a vector (x,y). As the spatial competition grows, the correlation between the distances becomes more apparent, reaching pseudo-long range for large Z. The hexagonal pattern arises due to the emergent self-organised compact packing of the centroids.

Structured phases with no translational order, such as the liquid or hexatic, present a qualitatively different $g(r)$ with damped oscillations appearing in the higher curves of Fig. 3. These oscillations result from strong exclusion interaction and represent the organisation of particles into "shells" or "waves" of neighbours. The location of the first of these peaks represents the threshold distance for which smaller separations are hindered by an effective hard core exclusion. As Z increases, the peak becomes narrower and its value grows and moves slightly to the right approaching 2σ, while an increasing number of progressively smaller peaks appear. Although the pair

correlation functions for the hexatic and liquid phases are qualitatively similar because angular differences are washed away, the increasing non-monotonic features are manifestation of an increasing order in the system as spatial competition grows. With even larger Z the geometrical arrangement of the particles break the radial pattern and the oscillations get distorted. The appearance of these distortions in the secondary peaks of $g(r)$ can be used as a discriminator for the onset of a solid phase as shown in studies on colloidal particle systems [26]. Additionally, when the system is in the solid phase, the oscillations in the pair correlation function become long lived and one talks about a quasi-long range order.

The emergent geometrical arrangement of the particles is even more evident in the 2D pair correlation function, as can be seen in fig 4. The exclusion interaction is isotropic for low spatial competition values, but a hexagonal pattern emerges for stronger competition. This is a natural consequence of the compact packing of the centroids, which breaks the radial symmetry of the system.

To identify precisely the parameter values at which different phases may appear, we identify proper order parameter in the system.

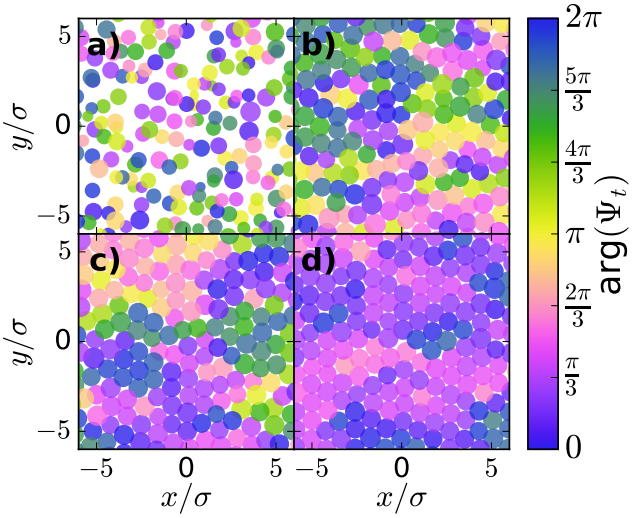

FIG. 5. (Color online) Translational order visualisation for the same system and corresponding competition parameters described in Fig. 4. The values of 0 or 2π indicate that a centroid is in a perfect crystalline lattice configuration.

LOCAL ORDER PARAMETERS

To characterize the territory translational symmetry in the solid phase it is convenient to use the local translational order parameter $\psi_t = \exp(-i\,\vec{G}\cdot\Delta\vec{r})$, with $\vec{G}$ the reciprocal centroid lattice vector and with $\Delta\vec{r}$ measuring the displacement of each particle from its ideal position in a crystalline lattice configuration. Fig. 5 shows an example of the translational order for different Z values, where each centroid has been coloured with the phase of its ψ_t value. Comparing the panels with increasing Z it is evident that only in the solid phase the spatial ordering does not decay away over distances.

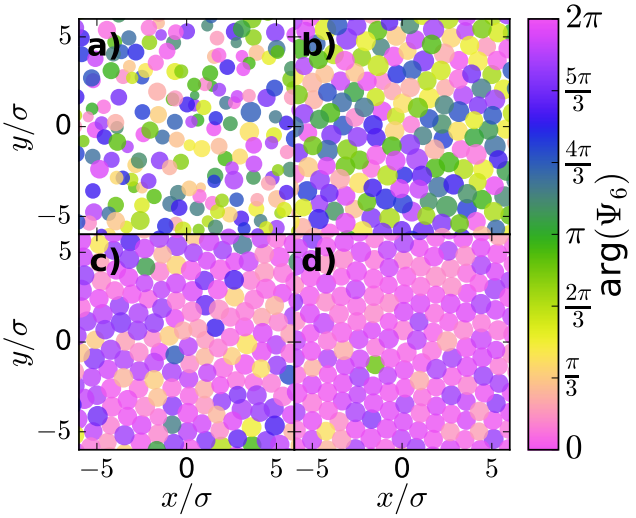

FIG. 6. (Color online) Bond orientational visualization for the same system and corresponding competition parameters described in Fig. 4. The values of 0 or 2π indicate that a centroid is arranged at the centre of an hexagonal geometry relative to all its nearest neighbours.

To distinguish the hexatic and liquid phases it is necessary to consider the so-called local bond-orientational order parameter [19] $\psi_6(\vec{r}) = \frac{1}{N_r}\sum_{j=1}^{N_r}\exp(6i\theta_j)$ with θ_j representing the angle made between a reference axis and the bond of the N_r nearest neighbours with the particle at $\vec{r}$. Fig. 6 shows the centroids in different phases where each centroid has been colored with the argument of their respective ψ_6, revealing that both the solid and hexatic phases have bond-orientational order.

GLOBAL ORDER PARAMETERS AND SUSCEPTIBILITIES

These translational and bond-orientational local order parameters can be used to build global order parameters, $\Psi_a = \sum_i \psi_a(\vec{r}_i)$, with $a = 6, t$, respectively. Panels (a) and (b) in Fig. 7 display the progressive appearance of the ordering process with the translational order rising sharply for high interaction, while the bond-orientational order increasing slowly along a wide range of Z values. To help establish precisely the Z parameter value where the liquid-hexatic and hexatic-solid phase transitions occur, a subblock analysis is used to try to overcome finite-size effects. We do this in Fig. 7(c,d) by plotting the susceptibilities $\chi_a = V(\langle|\Psi_a|^2\rangle - \langle|\Psi_a|\rangle^2)$ of the order parameters

as a function of Z for each subblock, where V represents the volume of the subblock.[29, 30] With a Z-resolution of 0.25, we identify the occurrence of the liquid-hexatic transition at $Z_h = 9.25$ and that of the hexatic-solid transition at $Z_s = 9.75$. These results were obtained using a perfect hexagonal tessellation as a initial condition and compared to a system that started with the walkers at random locations in space with no preliminary scent profile. The results agreed within the employed resolution.

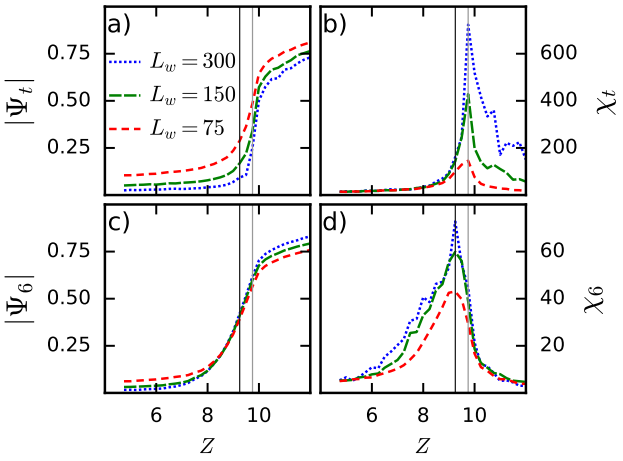

FIG. 7. (Color online) Bond-orientational and translational order parameters and their respective susceptibilities for a system of size 1200×1200 sites. To obtain the scaling the system was divided in n domains, with n =16, 64, and 256 respectively, so each window had a size of L^2/n . On the left, the order parameters display the ordering of the system and on the right the susceptibilities provide a quantitative way of estimating the location of the transition. The transition points, given by the vertical dark gray (orientational, Z_6) and light gray (translational, Z_T) lines, are $Z_6 = 9.25$ and $Z_T = 9.75$ respectively.

PHASE TRANSITIONS

According to the KTHNY theory of melting, the changes between phases liquid-hexatic and hexatic-solid occur via continuous phase transitions.[19] However, it has been shown that not all systems follow this scenario and thus the question arises on what type of transitions the system is experiencing. Recently, attention has been paid to the two-dimensional hard-disks system where the liquid-hexatic transition is claimed to be of first-order, breaking the KTHNY prediction [31, 32]. Interestingly enough, for similar systems, when the interaction between the disks is soft enough, the liquid-hexatic transition is again continuous [33].

The susceptibilities can be used to differentiate between first-order transitions and continuous ones.[30] In the former, the susceptibility should converge to a finite value, whereas in the latter it is divergent. The numerical data was not enough to unequivocally determine the divergence or convergence of the susceptibilities, although they were of the sufficient good quality to locate the transition points.

First-order transitions can be identified by a set of hallmarks, as for example a discontinuity or sharp increase in the order parameter, coexistence of phases and, for thermal systems, latent heat. We were unable to find any evidence of such hallmarks, despite conducting an extensive search for the coexistence of phases.

Therefore, the lack of evidence for a first-order transition points to a continuous liquid-hexatic transition. Nevertheless, it is always a possibility that the region of coexistence between the phases is very small and therefore was missed in the analysis or that the simulations were not large enough. Although plausible, a first-order transition would come as a surprise as the transitions are quite smooth and a continuous transition is consistent with the idea that the interaction between territories is substantially softer than that between hard disks.

GAS-LIQUID CROSSOVER IN THE TERRITORY CONFIGURATION AT SMALL Z

Prior to the melting transition, the system experiences another structuring process. For small Z territories are very small compared to the space free of foreign scent. As spatial competition increases (either by an increment in the active time T_A or a decrease in the specific volume ν), the scent-free space diminishes greatly and the territory boundaries are in constant overlap. The distance between neighbouring territories becomes more structured and one has a liquid. Similar to observations in Lennard-Jones and soft-sphere fluids in the supercritical region [34] we have no sharp transition but a simple crossover from a gas to a liquid phase.

A convenient way to charcaterize the change the system undergoes as competition increases for low value of Z is to plot the average territory size $\bar{S}$ normalised by ν' (see Eq. (B1)), where ν' is the size of the territories in a perfect geometrical arrangement. This number differs from the average number of sites available per animal ν because the sites at the boundary of each territory are shared between two or more agents (see appendix Fig. 10). Analogously to the analysis performed for the melting scenario in the main text we plot $\Psi_S = \bar{S}/\nu'$ and its associated variance χ_S in Fig. 8. At very low Z, either as a consequence of very short active times (low T_A) or very sparse populations (high ν), the territories are much smaller than the empty space that surrounds them. If Z is increased, the territories grow and display a bigger variety of shapes and χ_S increases. These features persist until the territories run out of space to grow and the interaction forces them to acquire more roundish shapes, decreasing χ_S. At very low Z the spatial competition

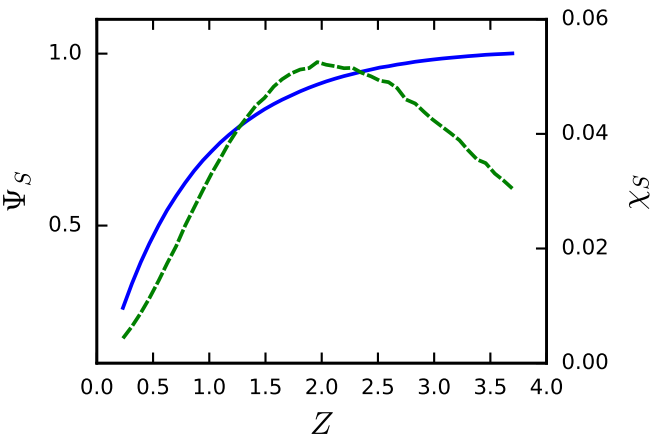

FIG. 8. (Color online) The normalised average territory size Ψ_S (solid line) and the standard deviation χ_S (dashed line) as a function of the spatial competition Z for a system of $L = 1200 \times 1200$ sites and $\nu = 48$. As spatial competition increases the mean territory size saturates to the maximum allowed value of the ordered phases, while the variance reaches zero asymptotically.

is not enough to cover the entire terrain and there are many sites left unmarked. As Z increases, the number of unmarked sites diminishes and Ψ_S asymptotically approaches one. The variance of the territory size increases first as a result of the more diverse shapes that bigger territories can acquire, but later on diminishes as a result of the exclusion interaction, which has a homogenising effect on the territory shape and size.

CONCLUSION

We have shown how to identify phases in an population of stigmergic interacting random walkers that leave a mark wherever they go and retreat upon encountering foreign marks. By using appropriate order parameters we have been able to find a cross-over between a gas and a liquid state at low density or low interaction strength. And for intermediate density or interaction our evidence so far points to continuous phase transitions from liquid to hexatic and from hexatic to solid following the KHTNY theory of melting.

Modifications of the TRW model are possible and it would be interesting to see how the phase transition scenario changes accordingly. A change that may be appropriate to study a broader range of animals is to have the probability of retreat upon encounter of a foreign scent not equal to 1. An implementation of such idea, proposed in ref. [14] is to link the probability of retreat to the age of the scent, becoming lower the older the scent. In such a case we would not expect to see a qualitative change in the melting transition scenario as evidence points already towards continuous phase transitions. Since a retreat probability less than one effectively implies reducing the interaction strength, we expect that the observed transitions will occur for increasingly bigger Z.

A direct application of our findings is to population ecology. Past use of this territorial model to movement data in a red fox population reported times for which the scent deposited by the animals remained active for around 5.1 and 3.7 days with approximate densities, respectively, of 5.3 and 1.2 km^{-2} [23]. The first and second values were extracted from observations in the '90s, respectively, before and after an epizootic of mange that decimated the fox population. Use of these parameters in our Z definition gives values for both cases within the liquid regime.

Identifying the phase of a population has implications not only for conservation biology but also from the management point of view, e.g. if the population is subject to an infectious disease. In such a case a priori knowledge of the phase of the population can help discern if the territorial units may help buffering the spread of the infection, e.g. in the solid or hexatic case when territory displacement is minimal. This study could in fact be exploited to study further animal disease ecology. By supplementing territorial random walkers with an infection status exchangeable upon encounters, it would be possible to build a framework to study disease spread in territorial populations [35].

We believe that our study has relevance also to other application areas. In swarm robotics it can be used to determine search and coverage efficiency of decentralised territorial algorithms [36]. Furthermore, the proposed coarse-graining procedure that links the non-Markov micro-description to a Markov meso-description is applicable to many other complex systems [37].

ACKNOWLEDGEMENTS

We ackonwledge discussions with Andrea Cavagna, Matthew Faulkner, Henrik J. Jensen, Sidney Redner, John Toner. AHR thanks the support from CONACyT (Scholarship 217403). AHR and LG acknowledges funding from EPSRC grants EP/M027546/1 and EP/I013717/1.

APPENDICES

Appendix A: Number of distinct visited sites by a random walker

The number of distinct sites visited by a random walker in hypercubic lattices for any number of dimensions has been studied in the past [38–40]. The analytic expressions in the asymptotic limit of large number of steps n

are:

$$\begin{aligned} 2D \quad & S_n = \pi n/\log(n) \\ 3D \quad & S_n = An \end{aligned} \tag{A1}$$

where A is a constant that depends on the lattice configuration. For bigger dimensions S_n is also linear in n. In the two-dimensional case, the top expression in Eq. (A1) converges too slowly. We find more convenient to work with the empirical expression

$$S_n = Cn^{0.91}, \tag{A2}$$

with C a constant dependent on the geometry of the lattice, namely $C = 0.67$ for the square lattice and $C = 0.73$ for the triangular lattice. From Fig. 9 it is evident that Eq. (A2) represents a better approximation in particular for small number of steps.

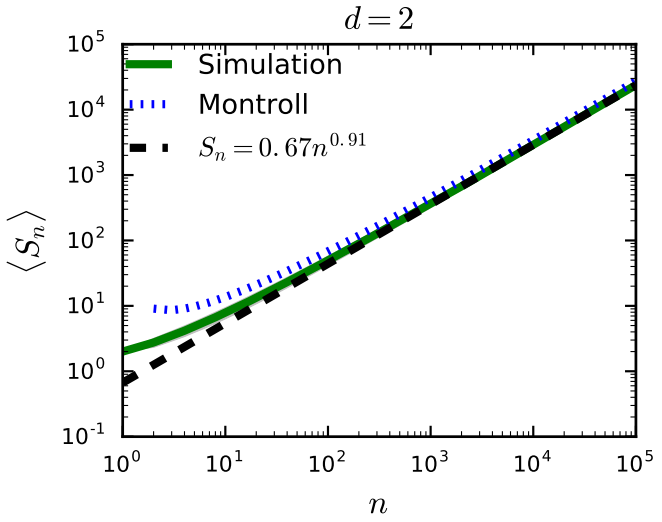

FIG. 9. (Color online) Time dependence of the number of distinct sites visited in a square lattice. The solid curve represents the numerical data averaged out of 10,000 independent realisations. The shaded region corresponds to the standard deviation from the mean. The match between the theoretical predictions in Eq. (A1) and simulation is great for all dimensions except for the two-dimensional case shown here, where the analytic prediction is off the mean by more than one standard deviation.

Appendix B: Geometrical properties of hexagonal territories

In a crystal configuration, the territories are hexagonal groups of lattice sites. The total number of sites ν' in a territory is given by the centered hexagonal number

$$\nu' = 3k(k-1) + 1, \tag{B1}$$

where k is a natural number that determines the maximum number of sites that are in straight line from the center of the hexagonal group to the edge of it, including the center itself. For example, in Fig. 10 the sites grouped by colour are hexagonal territories with 19 sites each and $k = 3$.

The sites at the border of a territory are shared between many walkers. To compute the average number of sites available per walker, ν, those sites with multiple occupancy must be weighted. The 6 corners of a territory are shared by 3 walkers and the $6(k-2)$ sites at the edges that are not corners are shared by 2 walkers each. Therefore, the average number of sites per walker ν is given by

$$\begin{aligned} \nu &= (3k(k-1)+1) - 6(k-2)/2 - 6(2/3) \\ &= 3(k-1)^2 \end{aligned} \tag{B2}$$

To connect with the parameters of the simulation, the definition of ν implies that it can be computed as

$$\nu = \frac{\text{number of sites}}{\text{number of walkers}}. \tag{B3}$$

This equation together with Eq. (B2) provides a way to compute the value k from simulation parameters, from which ν' can be computed.

Appendix C: Distance between territory centroids

If the distance between each site, that is black dot in Fig. 10, is set to 1, then the length of each edge of the corresponding hexagonal Voronoi cell is $1/\sqrt{3}$. In a

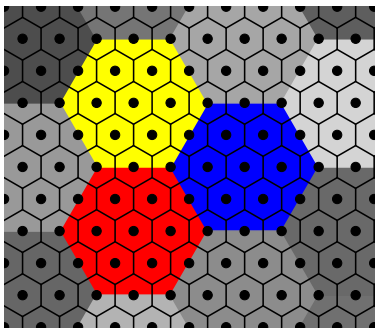

FIG. 10. (Color online) Schematic representation of a hexagonal tesselation of territories. Every dot represents a site in the lattice. The hexagonal black lines delimit the Voronoi cell of each site. Each territory has its own grey tonality (different colour in the online version) with the choice of the three central ones made to help better identify different territories visually. In this tesselation, the inverse of the density population is $\nu = 12$ and when corrected with the overlap between territories $\nu' = 19$. The distance between the centres of mass of two neighbouring territories is given by $\sqrt{\nu}$.

configuration like that displayed in Fig. 10, the vertical distance between rows is $\sqrt{3}/2$. There are $2(k-1)$ rows between the centers of two neighbours vertically aligned, so the distance 2σ between them is

$$\begin{aligned} 2\sigma &= 2(k-1)(\sqrt{3}/2) \\ &= \sqrt{\nu}, \end{aligned} \tag{A1}$$

where Eq. B2 has been used.

[1] D. D. Siljak, *Decentralized control of complex systems* (Dover publications, 2011).

[2] S. Camazine, J. L. Deneubourg, N. R. Franks, J. Sneyd, G. Theraulaz, and E. Bonabeau, *Self-organization in biological systems* (Princeton University Press, Princeton, USA, 2001).

[3] G. Theraulaz and E. Bonabeau, Artificial Life **5**, 97 (1999).

[4] P.-P. Grassé, Insec. Soc. **6**, 41 (1959).

[5] M. Dorigo, V. Maniezzo, and A. Colorni, IEEE T. Syst. Man. Cy. B **26**, 29 (1996).

[6] I. Kassabalidis, M. El-Sharkawi, R. Marks, P. Arabshahi, and A. Gray, in *Global Telecommunications Conference, 2001. GLOBECOM'01. IEEE*, Vol. 6 (IEEE, 2001) pp. 3613–3617.

[7] M. Allwright, N. Bhalla, H. El-faham, A. Antoun, C. Pinciroli, and M. Dorigo, in *International Conference on Swarm Intelligence* (Springer, 2014) pp. 158–169.

[8] R. Beckers, O. E. Holland, and J.-L. Deneubourg, in *Artificial Life IV*, edited by R. Brooks and P. Maes (MIT press, 1994) pp. 181–189.

[9] B. Hölldobler and E. O. Wilson, *Sociobiology: the new synthesis*, 2nd ed. (Springer, Berlin, 1998).

[10] L. M. Smith, A. L. Bertozzi, P. J. Brantingham, G. E. Tita, and M. Valasik, Discrete and Continuous Dynamical Systems **32**, 3223 (2012).

[11] P. R. Moorcroft and M. A. Lewis, *Mechanistic home range analysis* (Princeton University Press, Princeton, USA, 2006).

[12] L. Giuggioli and V. M. Kenkre, Move. Ecol. **2**, 20 (2014).

[13] J. R. Potts and M. a. Lewis, P. Roy. Soc. B-Biol. Sci. **281**, 20140231 (2014).

[14] L. Giuggioli, J. R. Potts, D. I. Rubenstein, and S. A. Levin, Proc. Natl. Acad. Sci. USA **110**, 16904 (2013).

[15] G. Grégoire and H. Chaté, Phys. Rev. Lett. **92**, 025702 (2004).

[16] M. Aldana, V. Dossetti, C. Huepe, V. M. Kenkre, and H. Larralde, Phys. Rev. Lett. **98**, 095702 (2007).

[17] T. Vicsek and A. Zafeiris, Phys. Rep. **517**, 71 (2012).

[18] T. Mora, A. M. Walczak, L. Del Castello, F. Ginelli, S. Melillo, L. Parisi, M. Viale, A. Cavagna, and I. Giardina, Nat. Phys. **12**, 1153 (2016).

[19] B. I. Halperin and D. R. Nelson, Phys. Rev. Lett. **41**, 121 (1978).

[20] D. J. Kosterlitz and J. M. Thouless, Journal of Physics C: Solid State Physics **1181**, 1181 (1973).

[21] A. P. Young, Phys. Rev. B **19**, 1855 (1979).

[22] L. Giuggioli, J. R. Potts, and S. Harris, PLoS Comput. Biol. **7**, e1002008 (2011).

[23] J. R. Potts, S. Harris, and L. Giuggioli, Am. Nat. **182** (2013).

[24] L. Giuggioli, G. Abramson, V. M. Kenkre, R. Parmenter, and T. L. Yates, J. Theor. Biol. **240**, 126 (2006).

[25] V. M. Kenkre, L. Giuggioli, and Z. Kalay, Phys. Rev. E **77**, 051907 (2008).

[26] Z. Wang, A. M. Alsayed, A. G. Yodh, Y. Han, Z. Wang, A. M. Alsayed, A. G. Yodh, and Y. Han, The Journal of Chemical Physics **15**, 154501 (2010).

[27] S. Asakura and F. Oosawa, J. of Polym. Sci. **33**, 183 (1958).

[28] K. Binder and W. Kob, *Glassy materials and disordered solids: An introduction to their statistical mechanics*, 2nd ed. (World Scientific, 2011).

[29] Y. Han, N. Ha, A. Alsayed, and A. Yodh, Physical Review E **77**, 041406 (2008).

[30] H. Weber, D. Marx, and K. Binder, Phys. Rev. B **51**, 14636 (1995).

[31] L. Berthier, H. Jacquin, and F. Zamponi, Phys. Rev. E **84**, 051103 (2011).

[32] M. Engel, J. A. Anderson, S. C. Glotzer, M. Isobe, E. P. Bernard, and W. Krauth, Phys. Rev. E **87**, 042134 (2013).

[33] S. C. Kapfer and W. Krauth, Phys. Rev. Lett. **114**, 035702 (2015).

[34] V. V. Brazhkin, Y. D. Fomin, A. G. Lyapin, V. N. Ryzhov, E. N. Tsiok, and K. Trachenko, Phys. Rev. Lett. **111**, 145901 1 (2013).

[35] L. Giuggioli, S. Pérez-Becker, and D. P. Sanders, Phys. Rev. Lett. **110**, 058103 (2013).

[36] L. Giuggioli, I. Arye, A. Heiblum Robles, and G. A. Kaminka, Proceedings of the 13th International Symposium on Distributed Autonomous Robotic Systems (DARS 2016) (2016 Accepted).

[37] Wayne M. Getz, Charles R. Marshall, Colin J. Carlson, Luca Giuggioli, Sadie J. Ryan, Stephanie S. Romañach, Carl Boettiger, Samuel D. Chamberlain, Laurel Larsen, Paolo D'Odorico, David O'Sullivan, Ecol. Lett. (Accepted 2017).

[38] A. Dvoretzky and P. Erdös, Proc. 2nd Berkeley Symp , 353 (1951).

[39] E. W. Montroll and G. H. Weiss, J. Math. Phys. **6**, 167 (1965).

[40] G. H. Vineyard, Journal of Mathematical Physics **4**, 1191 (1963).